

TABLE OF CONTENTS

COMMUNICATIONS

Atomic Force Microscopy of Slip Lines in FeAl

J.H. Schneibel, L. Martínez

In-Situ Imaging of μN Load Indents into GaAs

E.T. Lilleodden, W. Bonin, J. Nelson, J.T. WYROBEK, W.W. GERBERICH

Electrical and Photoconductive Properties of Boron-Doped Polycrystalline Diamond Films

W. Zhang, B. Hu, E. Xie, Y. Zhang, L. Han, Z. Song, G. Chen

In-Situ Single-Liquid-Source Metalorganic Chemical Vapor Deposition of $(\text{La}_{0.8}\text{Ca}_{0.2})\text{MnO}_3$ Giant Magnetoresistive Films

Y.Q. Li, J. Zhang, S. Pombrik, S. DiMascio, W. Stevens, Y.F. Yan, N.P. Ong

The Crystal Structure of the High Temperature Polymorph of α -Hexathieryl (α -6T/HT)

T. Siegrist, R.M. Fleming, R.C. Haddon, R.A. Laudise, A.J. Lovinger, H.E. Katz, P. Bridenbaugh, D.D. Davis

Dielectric Properties and Structure of Hydroxyapatite Ceramics Sintered by Different Conditions

J.J. Prieto Valdes, A. Victorero Rodriguez, J. Guevara Carrio

ARTICLES

Industrial Ecology—The Need to Re-Think the Materials Cycle: Some Problems, Solutions and Opportunities in the Materials Field

J. Szekely, G. Trapaga

Mechanical Properties of Biodegradable Soy-Protein Plastics

C.H. Schilling, T. Babcock, S. Wang, J. Jane

Texture and Transport in Spray Pyrolyzed $\text{TlBa}_2\text{Ca}_2\text{Cu}_3\text{O}_9$ Thick Films

J.E. Tkaczyk, J.A. Sutliff, J.A. DeLuca, P.J. Bednarczyk, C.L. Briant, Z.L. Wang, A. Goyal, D.M. Kroeger, D.H. Lowndes, E.D. Specht

Single Crystal Growth and Characterization of **$\text{Pb}_{0.5}\text{Sr}_{2.5}\text{Y}_{1-x}\text{Ca}_x\text{Cu}_2\text{O}_y$ System**

H. Jin, N.L. Wang, Y. Chong, M. Deng, L.Z. Cao, Z.J. Chen, G.E. Zhou, Z.W. Mao

Preparation of a-Axis $\text{YBa}_2\text{Cu}_3\text{O}_x$ Epitaxial Films Using Direct Current-95MHz Hybrid Plasma Sputtering

W. Ito

Origin of $\text{Y}_2\text{Ba}_1\text{Cu}_1\text{O}_5$ Free Region in Melt-Textured Y-Ba-Cu-O Oxides

C-J. Kim, H-G. Lee, K-B. Kim, G-W. Hong

Optimization of Y_2BaCuO_5 Phase Morphology for the Growth of Large Bulk YBCO Grains

F. Frangi, T. Higuchi, M. Deguchi, M. Murakami

Effects of Processing Parameters on the Levitation Force of Melt Processed $\text{YBa}_2\text{Cu}_3\text{O}_x$

C. Varanasi, P.J. McGinn, V. Pavate, E.P. Kvam

Growth of Ternary $\text{Si}_{1-x-y}\text{Ge}_x\text{C}_y$ Thin Films from a Single-Source Precursor, $\text{Ge}(\text{SiMe}_3)_4$

H-T. Chiu, C-S. Shie, S-H. Chuang

Mechanistic and Processing Studies in Combustion Synthesis of Niobium Aluminides

C.R. Kachelmyer, A.S. Rogachev, A. Varma

Copper-Alumina Materials Made by Infiltration in Boehmite

V. Pierre, D. Pierre, A.C. Pierre

Carbon Nitride Films Produced by High-Energy Shock Plasma Deposition

L.A. Bursill, P. JuLin, V.N. Gurarie, A.V. Orlov, S. Prawer

The Electrical Properties of $\text{La}_2\text{CuO}_4/\text{ZnO}$ Heterocontacts at Different Relative Humidities

E. Traversa, A. Bearzotti, M. Miyayama, H. Yanagida

Impedance Spectroscopy of Grain Boundaries in Nanophase ZnO

J. Lee, J-H. Hwang, J.J. Mashek, T.O. Mason, A.E. Miller, R.W. Siegel

Loss Spectra of Pure and La-Doped MgTiO_3 Microwave Ceramics

V.M. Ferreira, J.L. Baptista, J. Petzelt, G.A. Komandin, V.V. Voitsekhovskii

Identification of Oxidation Mechanisms in Silicon Nitride Ceramics by Transmission Electron Microscopy Studies of Oxide Scales

M. Backhaus-Ricoult, Yu.G. Gogotsi

The Synthesis and Characterization of Solid State Materials Produced by High Shear Hydrodynamic Cavitation

W.R. Moser, B.J. Marshik, J. Kingsley, M. Lemberger, R. Willette, A. Chan, J.E. Sunstrom IV, A. Boye

Chemistry, Microstructure, and Electrical Properties at Interfaces between Thin Films of Platinum and Alpha (6H) Silicon Carbide (0001)

L.M. Porter, R.F. Davis, J.S. Bow, M.J. Kim, R.W. Carpenter

Reaction Mediated Texturing of Barium Ferrite Magnetic Thin Films on ZnO Underlayer

J. Li, R. Sinclair, S.S. Rosenblum, H. Hayashi

A Comparison of C54-TiSi₂ Formation in Blanket and Submicron Complementary Metal Oxide Semiconductor Gate Structures Using In-Situ X-ray Diffraction During Rapid Thermal Annealing

L.A. Clevenger, R.A. Roy, C. Cabral, Jr., K.L. Saenger, S. Brauer, G. Morales, K.F. Ludwig, Jr., G. Gifford, J. Bucchignano, J. Jordan-Sweet, P. DeHaven, G.B. Stephenson

Gas Transport Model for Chemical Vapor Infiltration

T.L. Starr

Interfacial Reactions and Adhesion Strength of Metal/Ceramic Composites

H-F. Wang, W.W. Gerberich, J.E. Angelo

Absolute Measurement of Nanoscale Mechanical Properties of Graphite Using the Atomic Force Microscope

C.F. Draper, D.M. Schaefer, R.J. Colton, S.C. Webb, S.M. Hues

Structural Properties of Unconventional Lead Cuprate Glass

S. Hazra, A. Ghosh

Diffusion of Water in Silica Glass

R.H. Doremus

Improving Wettability of Polycarbonate (PC) and Adhesion with Aluminum by Ar⁺ Ion Irradiation

S-K. Koh, S-K. Song, W-K. Choi, H-J. Jung, S-N. Han

ABSTRACTS

COMMUNICATIONS

Atomic Force Microscopy of Slip Lines in FeAlJ.H. Schneibel*, L. Martinez⁺(*Oak Ridge National Laboratory, ⁺UNAM)

Fe-40 at.% Al-0.1 at.% B specimens were polished flat, strained at room temperature, and examined in an atomic force microscope. The angles of height contours perpendicular to the slip lines were interpreted as shear strains and were statistically evaluated. The frequency distributions of these shear strains correlated well with the macroscopic strains. The maximum shear strains found were not much larger than the macroscopic strains. In particular, no steep slip steps corresponding to large local shears were found.

Order No.: JA509-001

© 1995 MRS

In-Situ Imaging of μN Load Indents into GaAsE.T. Lilleodden*, W. Bonin*, J. Nelson*, J.T. Wyrobek⁺, W.W. Gerberich⁺(*University of Minnesota, ⁺Hysitron, Inc.)

Nanomechanical devices constitute an important and growing field, as they allow for new understanding of the mechanical properties at interfaces and surfaces. As an example, a newly developed nano-indentation device has been used to accomplish μN load indents into GaAs. First, it is shown that a plastic zone can be measured and is comparable to theory. Also, it is shown that the rate of indentation affects both the depth and upset zone of low load indents, implying a strain-rate sensitivity effect at room temperature. This is reinforced by observation of what appears to be a glide-based relaxation process.

Order No.: JA509-002

© 1995 MRS

Electrical and Photoconductive Properties of Boron-Doped Polycrystalline Diamond Films

W. Zhang, B. Hu, E. Xie, Y. Zhang, L. Han, Z. Song, G. Chen

(Lanzhou University)

The current-voltage (I-V) characteristics and time-dependence photoconductivity of the undoped and B-doped diamond films (DFs) before and after annealing were investigated. The boron and hydrogen concentration in diamond films was measured by means of nuclear reaction analysis (NRA) and elastic recoil detection (ERD) technique, respectively. The results show that induced boron atoms and hydrogen atoms affect the electrical and photoconductive properties of diamond films. During the annealing process, B concentration kept even but H content decreases. For undoped diamond films, the escaping H atoms have a great effect on the electrical characteristics, but for B-doped samples, this effect decreases with the increase of B concentration.

Order No.: JA509-003

© 1995 MRS

In-Situ Single-Liquid-Source Metalorganic Chemical Vapor Deposition of $(\text{La}_{0.8}\text{Ca}_{0.2})\text{MnO}_3$ Giant Magnetoresistive FilmsY.Q. Li*, J. Zhang*, S. Pombrik*, S. DiMascio*, W. Stevens*, Y.F. Yan⁺, N.P. Ong⁺(*Advanced Technology Materials, Inc., ⁺Princeton University)

A large magnetoresistance change ($\Delta R/R_H$) of -550% has been observed at 270 K in $(\text{La}_{0.8}\text{Ca}_{0.2})\text{MnO}_3$ thin films. The films were prepared *in-situ* on LaAlO_3 substrates by single-liquid-source metalorganic chemical vapor deposition. $\text{M}(\text{thd})_n$ (M=La, Ca, and Mn, and n=2,3) were dissolved together in an organic solution and used as precursors for the deposition of $(\text{La}_{0.8}\text{Ca}_{0.2})\text{MnO}_3$ thin films. Deposition was conducted at an oxygen partial pressure of 1.2 Torr and a substrate temperature ranging from 600°C to 700°C. The mechanism for the large magnetoresistance change in this manganese oxide is briefly discussed.

Order No.: JA509-004

© 1995 MRS

The Crystal Structure of the High Temperature Polymorph of α -Hexathienyl (α -6T/HT)

T. Siegrist, R.M. Fleming, R.C. Haddon, R.A. Laudise, A.J. Lovinger, H.E. Katz, P. Bridenbaugh, D.D. Davis

(*AT&T Bell Laboratories)

α -Hexathienyl (α -6T) is a highly promising material for application in thin film transistor devices. Recently, record high mobilities, together with record high current on/off ratios have been reported.¹ Thus far, structural information on this exciting material is sketchy. The crystal structures of several such hexamers have been investigated, but only with powder samples, since the crystal growth has proven exceedingly difficult.^{2,3,4,5} Powder Rietveld refinements on these materials are severely hampered by the large number of overlapping reflections, preferred orientation, ambiguities in symmetry, etc. Here, we present a crystal structure of the high temperature polymorph of α -6T (α -6T/HT), as determined from a single crystal structure analysis. In this polymorph, the hexamer crystallizes in the smallest unit cell so far reported for this material, but the molecule is flat. Extended Hückel theory (EHT) band structure calculations show that α -6T/HT is an indirect gap semiconductor, with the conduction band minimum at Y and the valence band maximum at Γ . The conduction and valence bands both show a remarkable degree of dispersion along X and Y for a molecular crystal. The electronic band structure of this material is strikingly similar to that of the two-dimensional organic superconductors based on bis(ethylenedithio)tetrathiafulvalene (ET), such as κ -(ET)₂Cu(NCS)₂.

Order No.: JA509-005

© 1995 MRS

Dielectric Properties and Structure of Hydroxyapatite Ceramics Sintered by Different Conditions

J.J. Prieto Valdes, A. Victorero Rodriguez, J. Guevara Carrio
(Universidad de La Habana)

Several conditions for hydroxyapatite ceramic preparation were used: sintering at 1150°C in air or under H₂O vapor flow, quenched in water at room temperature after sintering, or slow cooling inside the furnace. Depending on specific combinations of these preparation conditions, in the resulting ceramics there are observed significant differences in the phase composition and dielectric properties, ranging from capacitive to a semiconducting response. Comparison between the experimental x-ray diffraction patterns and those calculated by the Rietveld method show that during sintering in air, approximately 40% of hydroxyapatite is transformed to tricalcium phosphate. The XRD analysis shows that this transformation could be possible by the following process: Ca₁₀(PO₄)₆(OH)₂ = 2Ca₃(PO₄)₂ + Ca₂P₂O₇ + 2CaO + H₂O.
Order No.: JA509-006 © 1995 MRS

ARTICLES**Industrial Ecology—The Need to Re-Think the Materials Cycle: Some Problems, Solutions and Opportunities in the Materials Field**

J. Szekely, G. Trapaga
(Massachusetts Institute of Technology)

The main thrust of this paper is to define the concept of industrial ecology and to discuss how its principles may be utilized to reconsider the materials cycle. Simply put, ecological principles imply that we minimize waste during manufacture and ensure that the products are recycled at the end of their useful life. Such a re-thought materials cycle has to stress waste minimization and, at the same time, track energy flows and cost considerations simultaneously with the movement of the materials streams. In this paper, special attention is paid to recycling issues in metals production, municipal waste and also to recycling issues pertaining to electronic materials. Comments are made on the driving forces and the barriers to industrial ecology, including economics, regulation, management and education and on the international aspects of industrial ecology.
Order No.: JA509-007 © 1995 MRS

Mechanical Properties of Biodegradable Soy-Protein Plastics

C.H. Schilling, T. Babcock, S. Wang, J. Jare
(Iowa State University)

Experiments were performed to evaluate the room-temperature mechanical properties of soy-protein plastics that were compression-molded with varying concentrations of glycerin plasticizer. Specimens exhibited stiff and brittle behavior with good tensile strength reliability based on Weibull statistics analysis. Raising the glycerin concentration from zero to twenty percent progressively increased the tensile strain-to-failure from 1.1 to 1.8% and reduced the tensile strength from 42.1 to 23.6 MPa, the tangent modulus from 4.56 to 1.79 GPa, and the Rockwell hardness from R118.4 to R75.7. Ultrasonic measurements indicated that raising the glycerin concentration from zero to twenty percent increased Poisson's ratio from 0.348 to 0.409 and reduced the Young's Modulus from 7.01 to 5.4 GPa and the shear modulus from 2.5 to 1.8 GPa. Significant increases in the tensile strength and the strength reliability resulted from eliminating Griffith's flaws by sieving the press powder before compression molding. Rockwell hardness rapidly decreased upon immersing these plastics in water at 25°C, an effect which was pronounced for the glycerin containing specimens.
Order No.: JA509-008 © 1995 MRS

Texture and Transport in Spray Pyrolyzed TlBa₂Ca₂Cu₃O₉ Thick Films

J.E. Tkaczyk*, J.A. Sutliff*, J.A. DeLuca*, P.J. Bednarzyk*, C.L. Briant*, Z.L. Wang*, A. Goyal*, D.M. Kroeger†, D.H. Lowndes†, E.D. Specht*
(*General Electric Research and Development, †Oak Ridge National Laboratory)

The electron backscattering pattern technique has been applied to the microstructural investigation of Tl(1223) thick films formed by vapor-phase thallination of Ag containing Ba-Ca-Cu-oxide precursors. For samples grown on polycrystalline YSZ, considerable biaxial alignment is found in localized, multi grain regions as wide as 100 μm or more. However, on scales above 1 mm the overall texture remains only uniaxial with the c-axes (i.e. [001]) aligned perpendicular to the plane of the substrate. On single crystal KTaO₃, an epitaxial relationship is evident which persists to the surface of a three micron thick film. Modest variations in the processing protocol yield films containing grains oriented with the c-axis in the plane resulting in the degradation of transport properties. The data suggest a growth model in which sparse nucleation occurs at the substrate followed by rapid lateral crystallization.
Order No.: JA509-009 © 1995 MRS

Single Crystal Growth and Characterization of Pb_{0.5}Sr_{2.5}Y_{1-x}Ca_xCu₂O_y System

H. Jin, N.L. Wang, Y. Chong, M. Deng, L.Z. Cao, Z.J. Chen, G.E. Zhou, Z.W. Mao
(University of Science and Technology of China)

Two kinds of methods such as spontaneous nucleation from flux-free stoichiometric melt and CuO flux method have been used for the growth of Pb_{0.5}Sr_{2.5}Y_{1-x}Ca_xCu₂O_y single crystals. The morphologies, phases and compositions occurring in the crystals grown from the two kinds of methods were compared systematically. Optimum conditions for the growth of large 1212 phase single crystals are x=0.15, 0.25 and 0.35. The lattice parameters of the crystals with the 1212 phase were found to be increasing upon Ca-doping. The resistivity behavior of the PbSrYCaCuO single crystals with the 1212 phase both in the state of as-grown and after extended annealings under various oxygen partial pressure was also discussed briefly.
Order No.: JA509-010 © 1995 MRS

Preparation of a-Axis YBa₂Cu₃O_x Epitaxial Films Using Direct Current-95MHz Hybrid Plasma Sputtering

W. Ito
(Superconductivity Research Laboratory-ISTEC)

The dc-95MHz hybrid plasma magnetron sputtering has been newly developed for obtaining a-axis oriented YBa₂Cu₃O_x (YBCO) films with an excellent crystallinity. The crystallinity was found to be the best among the films reported so far; the full width at half maximum value of 0.027° in the rocking curve measurement through the film (200) diffraction peak and χ_{\min} of 2% estimated from the barium signal behind the surface peak in Rutherford backscattering (RBS) measurement using a 1 MeV He⁺ ion. The success in the excellent crystallinity was explained from the ion acceleration model at the ion sheath formed near the substrate surface considering the high ion density, which was revealed to be a characteristic of hybrid plasma. Almost perfect epitaxial growth was also confirmed by transmission electron microscopy. A characteristic grain boundary structure depending on the substrate was observed for the films on NdGaO₃ and SrTiO₃ substrates. Twist boundary is dominant for the film on NdGaO₃, while symmetrical tilt boundary and basal-plane-faced tilt boundary exclusively exist for the film on SrTiO₃. The microstructure of the film on SrTiO₃ is supposed to be

very resistive against the film relaxation. The strain relief was observed by RBS channeling spectra for the relatively high superconducting films. The results of Raman spectroscopy and RBS oxygen resonant measurements indicated that the oxygen content is not a critical parameter for determining the superconductivity of the a-axis oriented YBCO films but the oxygen ordering in the plane of Cu-O chain and the relief of the film strain are important for the improvement of T_c .

Order No.: JA509-011

© 1995 MRS

Origin of Y_2BaCuO_5 Free Region in Melt-Textured Y-Ba-Cu-O Oxides

C.-J. Kim, H.-G. Lee, K.-B. Kim, G.-W. Hong
(Korea Atomic Energy Research Institute)

In order to understand formation mechanism of Y_2BaCuO_5 free region microstructures concerning incongruent melting and peritectic reaction were studied in melt-textured Y-Ba-Cu-O oxides. It is found that spherical pores form during incongruent melting of $YBa_2Cu_3O_{7-y}$ phase into Y_2BaCuO_5 and a Ba-Cu-O liquid phase. As the melting goes on, liquid phase flows into the pores and then produces spherical liquid pockets containing a few Y_2BaCuO_5 particles. During slow cooling of the sample from the peritectic temperature to the temperature where $YBa_2Cu_3O_{7-y}$ phase is formed, the liquid pockets are converted into $YBa_2Cu_3O_{7-y}$ phase containing a few Y_2BaCuO_5 particles. Sometimes, remnant Ba-Cu-O liquid phase is present at the center part of the Y_2BaCuO_5 free regions due to the incomplete peritectic reaction. It is concluded that formation of spherical pores during incongruent melting of $YBa_2Cu_3O_{7-y}$ is responsible for the formation of the Y_2BaCuO_5 free regions.

Order No.: JA509-012

© 1995 MRS

Optimization of Y_2BaCuO_5 Phase Morphology for the Growth of Large Bulk YBCO Grains

F. Frangi, T. Higuchi, M. Deguchi, M. Murakami
(Superconductivity Research Laboratory-ISTEC)

YBCO samples were prepared using different types of precursor powders: quenched powders, or $YBa_2Cu_3O_{7-x}$ and Y_2BaCuO_5 commercial ones, with and without Pt addition. Two stoichiometries, corresponding to 0 and 40% molar excess of Y_2BaCuO_5 phase were adopted. The behavior of Y_2BaCuO_5 phase through thermal treatments, typical of melt processes, was observed by quenching the samples at various stages. $YBa_2Cu_3O_{7-x}$ grain growth kinetics was enhanced and liquid phase losses were limited by optimizing the morphology of Y_2BaCuO_5 phase in the partially melted state, with the simultaneous presence of round particles $\leq 1 \mu\text{m}$ and needle-like ones with very high aspect ratio. The optimized processing conditions were adopted, together with a seeding technique, to grow YBCO samples. At 77 K, a magnetic levitation force of 2.5 kg was measured for a sample with 18 mm diameter and magnetization critical current densities over 10^4 A/cm^2 were reached at 1 T.

Order No.: JA509-013

© 1995 MRS

Effects of Processing Parameters on the Levitation Force of Melt Processed $YBa_2Cu_3O_x$

C. Varanasi*, P.J. McGinn*, V. Pavate*, E.P. Kvam*
(*University of Notre Dame, *Purdue University)

Melt processing of $YBa_2Cu_3O_x$ (Y-123) with a $NdBa_2Cu_3O_x$ -123 single crystal seed has been used to grow large single grain Y-123 samples. Processing parameters have been varied to observe the resulting differences in the levitation force of the samples. Increased hold time above the peritectic temperature and increased undercooling temperature have been observed to be beneficial in enhancing the levitation force of the samples. The levitation force measurements have been correlated with magnetization measurements on the crushed domains.

Order No.: JA509-014

© 1995 MRS

Growth of Ternary $Si_{1-x}Ge_xC_y$ Thin Films from a Single-Source Precursor, $Ge(SiMe_3)_4$

H.-T. Chiu, C.-S. Shie, S.-H. Chuang
(National Chiao Tung University)

$Ge(SiMe_3)_4$ was used as a single-source precursor to deposit thin films of alloys of germanium, silicon and carbon, $Si_{1-x}Ge_xC_y$, by low pressure chemical vapor deposition on silicon substrates at temperatures 873–973 K. X-ray diffraction studies indicated that the films grown above 898 K were cubic phase ($a=0.441\text{--}0.442 \text{ nm}$). Infrared spectra of the films showed a major absorption near 783 cm^{-1} . X-ray photoelectron spectra of a typical thin film showed binding energies of Ge_{3d} , Si_{2p} , and C_{1s} electrons at 30.0, 100.6 and 283.2 eV, respectively. As determined by wavelength dispersive spectroscopy, x was 0.07–0.15 and y was 0.43–0.50, indicating that the films contained 7–15% Ge, 38–43% Si and 43–50% C. At 973 K, C/(Si + Ge) ratio was 1. Based on these data, the films deposited above 898 K have a structure of β -SiC with Ge atoms replacing some Si atoms in the lattice.

Order No.: JA509-015

© 1995 MRS

Mechanistic and Processing Studies in Combustion Synthesis of Niobium Aluminides

C.R. Kachelmyer, A.S. Rogachev, A. Varma
(University of Notre Dame)

Combustion synthesis of $NbAl_3$ and Nb_2Al was studied using the volume combustion mode. The effects of heating rate and green density were examined for $NbAl_3$ synthesis. The effect of green density was also investigated for Nb_2Al . Greater reaction completion was achieved at higher heating rates and green densities. In both $NbAl_3$ and Nb_2Al samples, the reaction was initiated above the melting point of Al. Quenching ($Nb+3Al$) samples pressed at relatively high and low densities below the ignition temperature, and results of a particle-foil experiment, identified the spreading characteristic of molten Al over Nb, providing mechanistic details about niobium aluminide product formation.

Order No.: JA509-016

© 1995 MRS

Copper-Alumina Materials Made by Infiltration in Boehmite

V. Pierre, D. Pierre, A.C. Pierre
(The University of Alberta)

New materials were made by infiltration of sol-gel boehmite thin films with copper acetate. The structure and phase transformation of these materials during heat treatment was studied. It was found that infiltration in the boehmite state did not end up in the same material as direct infiltration in the θ -alumina derived from boehmite, even after both types of materials were heat treated at 900°C . Infiltration in boehmite makes it possible to synthesize sandwich structures composed of alternate layers of CuO and of γ -alumina.

Order No.: JA509-017

© 1995 MRS

Carbon Nitride Films Produced by High-Energy Shock Plasma Deposition

L.A. Bursill, P. JuLin, V.N. Gurarie, A.V. Orlov, S. Prawer
(The University of Melbourne)

High-energy shock plasma deposition techniques are used to produce carbon nitride films containing both crystalline and amorphous components. The structures are examined by high-resolution transmission electron microscopy, parallel-electron-energy loss spectroscopy and electron diffraction. The crystalline phase appears to be face-centered cubic with unit cell parameter approximately $a=0.63 \text{ nm}$ and it may be stabilized by calcium and oxygen at about 1–2 at.% levels. 85 at.% of the carbon atoms appear to have trigonal bonding for the crystalline phase; the remaining 15 at.% having tetrahedral bonding. The amorphous carbon-nitride film component varies from essentially nanocrystalline graphite, containing virtually no nitrogen, to amorphous carbon-nitride containing up to 10 at.% N, where the fraction of sp^3 bonds ranges up to approximately 85 at.%. There is PEELS evidence that the nitrogen atoms have sp^2 trigonal bonds in both the amorphous and crystalline phases.

Order No.: JA509-018

© 1995 MRS

The Electrical Properties of La₂CuO₄/ZnO Heterocontacts at Different Relative HumiditiesE. Traversa*, A. Bearzotti[†], M. Miyayama[#], H. Yanagida[#]
(*Università di Roma "Tor Vergata," [†]C.N.R., [#]University of Tokyo)

The humidity sensing electrical properties of heterocontacts between p-type La₂CuO₄ and n-type ZnO semiconductors, and of the single oxides, as a comparison, were studied. The heterocontacts were prepared by mechanically pressing sintered discs of the two oxides. The electrical characterization of the heterocontacts was carried out using d.c. and a.c. measurements at various relative humidity (RH) values, in order to evaluate the sensing mechanism and the electrical properties of these p-n junctions. Their humidity sensitivity was explained in terms of the variation of the barrier height at the p-n junctions, due to the saturation of the original interface states by physisorbed water, which leads to the release of trapped electrons, resulting in an increase in the forward current. The higher the number of interface states, the higher the RH-sensitivity of the heterocontacts. Electrochemical impedance spectroscopy (EIS) measurements showed, at 90% RH, a distribution of capacitances with different relaxation times, which may be caused by the electrolysis of water molecules at p-n junction sites. For their use as humidity sensors, they showed a response of 4 orders of magnitude in the whole RH range tested, and a fast response time. The response of the heterocontacts was bias-dependent, tunable by externally applied electric field. They also have stand-by capability, and a self cleaning mechanism, which allow them to be described as intelligent materials.

Order No.: JA509-019

© 1995 MRS

Impedance Spectroscopy of Grain Boundaries in Nanophase ZnOJ. Lee*, J.-H. Hwang[†], J.J. Mashek[†], T.O. Mason[†], A.E. Miller*, R.W. Siegel[#](*University of Notre Dame, [†]Northwestern University, [#]Argonne National Laboratory)

Sintered compacts of nanophase ZnO (~60 nm average grain size, presintered at 600°C) were made from powders (~13 nm) prepared by the gas-condensation technique. Impedance spectra were taken as a function of temperature over the range 450–600°C and as a function of oxygen partial pressure over the range 10⁻³–1 atm (550 and 600°C only). The activation energy was determined to be 55 kJ/mole (0.57 eV) and was independent of oxygen partial pressure. The oxygen partial pressure exponent was -1/6. Impedance spectra exhibited nonlinear I-V behavior, with a threshold of approximately 6 V. These results indicate that grain boundaries are governing the electrical properties of the compact. Ramifications for oxygen sensing and for grain boundary defect characterization are discussed.

Order No.: JA509-020

© 1995 MRS

Loss Spectra of Pure and La-Doped MgTiO₃ Microwave CeramicsV.M. Ferreira*, J.L. Baptista*, J. Petzelt[†], G.A. Komandin[†], V.V. Voitsekhovskii[†](*Universidade de Aveiro, [†]Czech Academy of Sciences)

Pure and La-doped magnesium titanate (MgTiO₃) microwave ceramics were sintered and structurally and dielectrically characterized. Doping provides small inclusions of a second phase found to correspond to the La₂Ti₂O₇ compound. It increases the microwave dielectric loss appreciably and gives rise to three absorption peaks in the submillimeter range assigned to polar phonons of the La₂Ti₂O₇ structure. This assignment was confirmed by a direct reflectivity measurement on La₂Ti₂O₇ ceramics. From the temperature dependence of submillimeter losses in the pure sample, one can estimate that from 1000 down to at least 8 GHz about half of the room temperature losses are intrinsic, i.e., due to two-phonon absorption processes.

Order No.: JA509-021

© 1995 MRS

Identification of Oxidation Mechanisms in Silicon Nitride Ceramics by Transmission Electron Microscopy Studies of Oxide ScalesM. Backhaus-Ricoult*, Yu.G. Gogotsi[†]
(*CNRS, [†]University of Oslo)

Additive-free HPSN and Y₂O₃+Al₂O₃-doped HPSN are oxidized in air in the temperature range from 1300 to 1500°C. TEM, SEM, EDS and XRD are used to analyze the composition and microstructure of the oxide scales in order to determine the oxidation mechanisms.

HPSN exhibits excellent resistance to oxidation in air at temperatures up to 1480°C due to the formation of a protective silica (cristobalite) scale. No formation of Si₂N₂O and oxygen enriched β' Si₃N₄ under the silica layer is observed for materials densified without additives.

Oxidation rates of additive-containing HPSN are more important due to the formation of a viscous aluminosilicate phase, which easily penetrates along the grain boundaries in the material. Silicon nitride grains in contact with the viscous phase first become enriched in aluminum and oxygen and are then dissolved in the glassy phase. No Si₂N₂O intermediate layer is formed. The finding of the decisive role of the aluminosilicate in the oxidation process allows to explain inconsistencies observed in the oxidation kinetics of silicon nitride ceramics. Effects of sintering additives, WC contamination and temperature on the oxidation mechanisms and structure of oxide scales are discussed.

Order No.: JA509-022

© 1995 MRS

The Synthesis and Characterization of Solid State Materials Produced by High Shear Hydrodynamic CavitationW.R. Moser, B.J. Marshik, J. Kingsley, M. Lemberger, R. Willette, A. Chan, J.E. Sunstrom IV, A. Boye
(Worcester Polytechnic Institute)

A new method for the synthesis of complex metal oxides, based on hydrodynamic cavitation, was used to prepare pure phase, nano-structured solid state materials. The continuous process afforded a wide variety of metal oxides in grain sizes of 1–10 nm. Catalysts, ceramics, superconductors, piezoelectrics, and zeolites were prepared by cavitation synthesis. The method enabled the synthesis of fine particles of metals and metal oxides supported on high surface area supports such as silica, and the synthesis of fine particles of cubic zirconia without ion modification.

Order No.: JA509-023

© 1995 MRS

Chemistry, Microstructure, and Electrical Properties at Interfaces between Thin Films of Platinum and Alpha (6H) Silicon Carbide (0001)L.M. Porter*, R.F. Davis*, J.S. Bow[†], M.J. Kim[†], R.W. Carpenter[†]
(*North Carolina State University, [†]Arizona State University)

Thin films (4–1000 Å) of Pt were deposited via UHV electron beam evaporation at room temperature on monocrystalline, n-type α (6H)-SiC (0001) substrates and examined in terms of chemistry, microstructure, and electrical properties. The as-deposited contacts were polycrystalline and showed excellent rectifying behavior with low ideality factors (n < 1.1) and leakage currents of 5x10⁻⁸ A/cm² at -10 V. The Schottky barrier height increased from 1.06 eV before annealing to 1.26 eV after successive 20 min. anneals at 450, 550, 650, and 750°C. In addition, the leakage currents decreased to 2x10⁻⁸ A/cm² at -10 V. Interfacial reactions were not observed at annealing temperatures below 750°C; above this temperature, Pt₂Si and C precipitates were identified in the reaction zone.

Order No.: JA509-024

© 1995 MRS

Reaction Mediated Texturing of Barium Ferrite Magnetic Thin Films on ZnO Underlayer

J. Li⁺, R. Sinclair^{*}, S.S. Rosenblum⁺, H. Hayashi⁺
 (*Stanford University, ⁺Kobe Steel USA Inc.)

Using facing target sputtering, crystalline magnetoplumbite-type barium ferrite (BaFe₁₂O₁₉ or BaM) thin films have been prepared *in-situ* at a substrate temperature of 640°C without post-deposition annealing. Using our facing target sputtering system, BaM thin films grow randomly if they are directly deposited onto Si or thermally oxidized Si substrates. However, deposited onto a sputtered ZnO layer (~230 Å) on Si substrates, BaM thin films show excellent c-axis out-of-plane texture with a 0.2° c-axis dispersion angle, as indicated by x-ray diffraction (XRD). Cross-section transmission electron microscopy (XTEM) reveals that the textured films epitaxially grow on a transition layer, which is formed between BaM and ZnO. No direct epitaxial relation between BaM and ZnO was observed. This transition layer is identified by TEM and XRD as ZnFe₂O₄, which, from a structure point of view, reduces the lattice mismatch between BaM and ZnO, and also enhances the c-axis out-of-plane epitaxial growth. ZnFe₂O₄ is a reaction product of BaM and ZnO as indicated by both TEM and XRD. After *ex-situ* annealing the film in air at 800°C, the ZnFe₂O₄ layer becomes thicker at the expense of BaM and ZnO. The lattice parameters of both BaM and ZnO decreased as annealing time increased.

Order No.: JA509-025

© 1995 MRS

A Comparison of C54-TiSi₂ Formation in Blanket and Submicron Complementary Metal Oxide Semiconductor Gate Structures Using In-Situ X-ray Diffraction During Rapid Thermal Annealing

L.A. Clevenger^{*}, R.A. Roy^{*}, C. Cabral, Jr.^{*}, K.L. Saenger^{*}, S. Brauer^{*}, G. Morales⁺, K.F. Ludwig, Jr.⁺, G. Gifford[#], J. Bucchignano⁺, J. Jordan-Sweet^{*}, P. DeHaven[#], G.B. Stephenson^{*}
 (*IBM T.J. Watson Research Center, ⁺Boston University, [#]IBM Microelectronics Division)

We demonstrate the use of a synchrotron radiation source for *in-situ* x-ray diffraction analysis during rapid thermal annealing (RTA) of 0.35 μm Salicide (self aligned silicide) and 0.4 μm Polycide (silicided polysilicon) TiSi₂ complementary metal oxide semiconductor (CMOS) gate structures. It is shown that the transformation from the C49 to C54 phase of TiSi₂ occurs at higher temperatures in submicron gate structures than in unpatterned blanket films. In addition the C54 that forms in submicron structures is (040) oriented while the C54 that forms in unpatterned Salicide films is randomly oriented. Although the preferred orientation of the initial C49 phase was different in the Salicide and Polycide gate structures, the final orientation of the C54 phase formed was the same. An incomplete conversion of C49 into C54-TiSi₂ during the RTA of Polycide gate structures was observed and is attributed to the retarding effects of phosphorus on the transition.

Order No.: JA509-026

© 1995 MRS

Gas Transport Model for Chemical Vapor Infiltration

T.L. Starr
 (Georgia Institute of Technology)

A node-bond percolation model is presented for the gas permeability and pore surface area of the coarse porosity in woven fiber structures during densification by chemical vapor infiltration (CVI). Model parameters include the number of nodes per unit volume and their spatial distribution, and the node and bond radii and their variability. These parameters relate directly to structural features of the weave. Some uncertainty exists in the proper partition of the porosity between "node" and "bond" and between intra-tow and inter-tow, although the total is constrained by the known fiber loading in the structure. Applied to cloth layup preforms the model gives good agreement with the limited number of available measurements.

Order No.: JA509-027

© 1995 MRS

Interfacial Reactions and Adhesion Strength of Metal/Ceramic Composites

H-F. Wang^{*}, W.W. Gerberich⁺, J.E. Angelo[#]
 (*University of Florida, ⁺University of Minnesota, [#]Sandia National Laboratories)

The interfacial fracture energy of Ti/Al₂O₃ composites was measured with and without a diffusion barrier at different bonding temperatures by using four point bending tests. It was found that the interfacial fracture energy increases with increasing bonding temperature up to 950°C. When the bonding temperature was further raised to 1000°C, the interfacial fracture energy drops. The decrease of the interfacial fracture energy is due to the formation of the continuous intermetallic compound, Ti₃Al at the interface between Ti and Al₂O₃. By using a diffusion barrier, the interfacial fracture energy decreases from 25.4 to near 0 J/m² and 32.9 to 8.7 J/m² for applied bonding temperatures of 800 and 900°C, respectively. This is because the diffusion barrier reduced the diffusion of Al across the interface and into the Ti, thereby preventing a strong chemical bond at the interface. For the composite bonded at 900°C, the crack propagation was found to occur at the interface between the Ti and Al₂O₃. The interfacial failure was found to be in the Ti₃Al reaction layer for the composite processed at 1000°C. With a diffusion barrier, the crack propagation path follows several interfaces. Evaluation of the processing temperature on the mechanical properties of the Ti was also obtained by using a nanoindentation technique.

Order No.: JA509-028

© 1995 MRS

Absolute Measurement of Nanoscale Mechanical Properties of Graphite Using the Atomic Force Microscope

C.F. Draper^{*}, D.M. Schaefer⁺, R.J. Colton⁺, S.C. Webb[#], S.M. Hues⁺
 (*Vanderbilt University, ⁺Naval Research Laboratory, [#]Wilson Instruments/Instron Corporation)

Nanoindentation involves measuring the mechanical properties of a surface with a tip/surface contact area or a penetration depth on the nanometer scale. In this work, the absolute value of elastic modulus and hardness are measured, using an atomic force microscope, for the surface of highly oriented pyrolytic graphite (HOPG) as a function of penetration depth and strain. These values were then verified using the UMIS-2000 indentation instrument. The elastic modulus and Meyer hardness of HOPG increases with strain with the bulk modulus being reached at a true strain of 0.01. A model explaining the dependence of modulus and hardness on penetration depth is presented which invokes the effects of interbasal layer tensile strain produced by exfoliation of the HOPG surface during sample preparation.

Order No.: JA509-029

© 1995 MRS

Structural Properties of Unconventional Lead Cuprate Glass

S. Hazra, A. Ghosh
 (Indian Association for the Cultivation of Science)

Glass formation and structural properties of the unconventional lead cuprate glasses of compositions (CuO)_x(PbO)_{100-x} (mol.%) have been reported for the first time. X-ray diffraction and electron microscopic studies show that the glass formation occurs for x=15–50 mol.%. The compositional dependence of the density, molar volume and glass transition temperature suggests that all glass compositions in this domain have the same topology and network connectivity. The glass structure is built up of [PbO₄] tetrahedral units. On heat treatment above glass transition temperatures, the glasses crystallize to CuO and PbO. Electron spin resonance (ESR) spectra of the glass compositions consist of broad resonance lines.

Order No.: JA509-030

© 1995 MRS

Diffusion of Water in Silica Glass

R.H. Doremus

(Rensselaer Polytechnic Institute)

The diffusion of water into silica glass is modeled to result from the diffusion of molecular water into the glass and its reaction with the silicon-oxygen network to form SiOH groups. Equations for this diffusion-reaction mechanism are presented and compared with experimental diffusion profiles. At temperatures above about 500°C the reaction goes to equilibrium, but at lower temperatures it does not, leading to a time dependence of the concentration of surface reacted OH groups and of their apparent diffusion coefficient. At higher temperatures, the OH groups are nearly immobile, but diffuse far enough to sample neighboring OH groups, leading to a bimolecular reverse reaction. At lower temperatures only OH pairs react; giving a first-order reaction. When water tagged with O^{18} diffuses into silica, the O^{18} exchanges with O^{16} in the silicon-oxygen network of the glass. This process is also controlled by the rate of diffusion of molecular water into the glass, and the rate of O^{18} - O^{16} exchange. This diffusion-reaction mechanism gives a unified description of the diffusion of water in silica glass from 160° to 1200° at least.

Order No.: JA509-031

© 1995 MRS

Improving Wettability of Polycarbonate (PC) and Adhesion with Aluminum by Ar⁺ Ion Irradiation

S-K. Koh*, S-K. Song*, W-K. Choi*, H-J. Jung*, S-N. Han*

*(*Korea Institute of Science and Technology, ⁺Aju Engineering)*

Improving wettability of PC surface to triple distilled water has been carried out by Ar⁺ ion irradiation with blowing oxygen gas. Amount of Ar⁺ was changed from 10^{14} to 5×10^{16} ions/cm² at 1 keV energy by Kaufman type ion source. Contact angle of the water to PC has been reduced from 78° to 50° with Ar⁺ irradiation, and to 12° with Ar⁺ irradiation in various vacuum pressures adjusted by oxygen gas flow rate (0-4 sccm). Strong O-H stretching vibration peaks at around 3370 cm⁻¹ on FT-IR spectra of the polymer appeared after the surface treatments, and the wetting angle of the treated PC was returned to 78° when the PC was exposed in an air environment. The minimum contact angles were maintained with the same value when the irradiated polymers were kept in dilute HCl solution. The improved wettability and surface chemical reaction by Ar⁺ ion irradiation with oxygen was explained in view of formation of a hydrophilic functional group. Enhanced adhesion between aluminum and PC was conformed by scotch tape test, and was discussed with relation between hydrophilic group on the polymer surface and the deposited metal.

Order No.: JA509-032

© 1995 MRS

Please use the convenient postcard located in the back of the *MRS Bulletin* to order *JMR* reprints.

When ordering single article reprints please note they are not available until the issue is published.

PUBLICATION DATE: AUGUST 18
SPECIAL PREPUB PRICING UNTIL AUGUST 1, 1995
SO ORDER NOW AND SAVE!

Handbook of Modern Ion Beam Materials Analysis

Editors: Joseph R. Tesmer, Michael Nastasi

Contributing Editors: J. Charles Barbour, Carl J. Maggiore, and James W. Mayer

The *Handbook of Modern Ion Beam Materials Analysis* is a compilation of updated techniques and data for use in the ion-beam analysis of materials. The information presented is unavailable collectively from any other source, and places a strong emphasis on practical examples of the analysis techniques as they are applied to common problems.

The book's 13 chapters cover discussions and examples, while 18 appendices provide extensive compilations of relevant data. Numerous techniques are discussed, including elastic recoil detection and activation analysis. Material in the book pushes the boundaries of ion-beam analysis to higher energies. The detection of light elements is emphasized, and background materials in the areas of energy loss, nuclear theory, instrumentation, analysis pitfalls and radiation safety are also provided for a better understanding of the principles basic to the techniques.

ISBN: 1-55899-254-5

Code: IBH-B

Special Prepub Prices
(before August 1, 1995)Standard Prices
(after August 1, 1995)

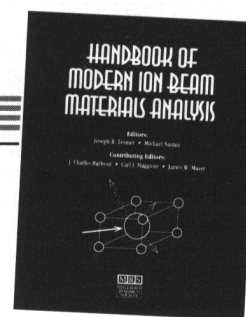
\$125.00 MRS Members
 \$160.00 U.S. List
 \$185.00 Foreign

\$160.00 MRS Members
 \$200.00 U.S. List
 \$230.00 Foreign

**Order
From:**



MATERIALS RESEARCH SOCIETY
 Publications Department
 9800 McKnight Road
 Pittsburgh, PA 15237-6006 U.S.A.
 Phone: 412-367-3012 Fax: 412-367-4373

**Chapters**

1. Introduction
2. Energy Loss
3. Nuclear Theory
4. Backscattering
5. Elastic Recoil Detection
6. Nuclear Reaction Analysis: Particle - Particle
7. Nuclear Reaction Analysis: Particle - Gamma
8. Nuclear Reactions for Hydrogen Analysis
9. Charged Particle Activation Analysis
10. Channeling
11. Instrumentation and Laboratory Practice
12. Pitfalls in Ion Beam Analysis
13. Radiation Safety

Appendices

1. Elements
2. Physical Constants, Conversions, and Useful Combinations
3. Stopping and Range
4. Scattering and Reaction Kinematics
5. K Factors for RBS
6. RBS Rutherford Cross Sections
7. Non-Rutherford Cross Sections
8. Actual Coulomb Barriers
9. Elastic Recoil Detection Data
10. Particle - Nuclear Reaction Parameters
11. Particle - Particle Cross Sections
12. Particle - Gamma Nuclear Reaction Analysis
13. Hydrogen Nuclear Reaction Analysis
14. Activation Analysis Data
15. Channeling Data
16. Thin-Film Materials and Preparation
17. Accelerator Energy Calibration Data & Stability
18. Radiation Hazards of (α, n) Reactions

950126A